

Composition Dependence of the Photochemical reduction of Ag by $\text{Ba}_{1-x}\text{Sr}_x\text{TiO}_3$

Abhilasha Bhardwaj, Nina V. Burbure, Andrew Gamalski,[†] and Gregory S. Rohrer*

Department of Materials Science and Engineering, Carnegie Mellon University, Pittsburgh, Pennsylvania 15213. [†]Current address: Physics Department, Arizona State University, Mesa, AZ 85212.

$\text{Ba}_{1-x}\text{Sr}_x\text{TiO}_3$ solid solutions with $x = 0-1$ were used to photochemically reduce aqueous Ag^+ to Ag^0 . The reduction of Ag on BaTiO_3 is spatially selective and correlated to the locations of positive ferroelectric domains. On SrTiO_3 , silver reduction is spatially uniform. As strontium is added to BaTiO_3 , there is a continuous change from spatially localized to uniform reactivity that is complete at $x > 0.27$. The relative heights of the silver deposits, as measured by atomic force microscopy, were used to quantify the relative reactivities. A local maximum in the reactivity is observed at $x = 0.26$, which is near the cubic-tetragonal phase boundary. The change from spatially selective to spatially uniform reactivity is associated with decreased polarization as the strontium concentration increases. The local maximum in reactivity near the phase boundary is associated with an anomalously high dielectric constant at this composition that enlarges the space-charge region. The results are consistent with the idea that the width of the space-charge region is an important factor in determining the photochemical reactivity.

1. Introduction

When illuminated by ultraviolet (UV) light, metal oxide surfaces are able to catalyze the dissociation of water into hydrogen into oxygen; as a result, they have been studied extensively as potential catalysts to synthesize hydrogen fuel.¹⁻³ However, the efficiency with which absorbed light is converted to usable hydrogen is limited by the recombination of charge carriers and the back reaction of intermediate species to reform water.^{3,4} Therefore, mechanisms to separate the charge carriers and spatially isolate the oxidation and reduction reactions are of interest because they might be controlled to improve efficiency.

Polar oxides with internal dipolar fields are able to internally separate photogenerated carriers via the bulk photovoltaic effect.⁵⁻⁷ Photochemical experiments on BaTiO_3 have shown that reduction reactions (for example, the reduction of Ag^+ to Ag^0) are favored on the surfaces of domains with the positive polarization directed toward the surface and oxidation reactions (for example, the oxidation of Pb^{2+} to Pb^{4+}) are favored on the opposite domains.⁸⁻¹⁰ Similar effects have been observed on lead zirconate titanate and LiNbO_3 , and this is the basis of the process known as ferroelectric nanolitho-

graphy.¹¹⁻¹⁴ The spatial localization of the reaction is interpreted using the energy level diagrams in Figure 1, which illustrate the assumed band bending for different domains of BaTiO_3 in aqueous solution.

The energy level diagrams in Figure 1 are drawn with reference to the standard hydrogen electrode scale, assuming that (i) the band gap of BaTiO_3 is 3.2 eV,^{15,16} (ii) the conduction band potential (E_C) is close to 0 V,¹⁷ and (iii) it is n -type with donor states a few tenths of a volt below the conduction band edge that determine the Fermi level (E_F).¹⁸ It is further assumed that, for a neutral domain (for example, when the domain polarization vector is perpendicular to the surface normal) there will be a small amount of upward band bending in a solution with a pH near 7, as illustrated in Figure 1b. For domains in which the positive end of the polarization vector points toward the surface (positive domains), we assume that the positive charge draws compensating electrons toward the surface and either reduces the band bending on the neutral surface or even bends the bands downward, as shown in Figure 1a. The opposite occurs on negative domains, where the polarization repels electrons from the surface and bends the bands further upward with respect to the neutral surface.

*Author to whom correspondence should be addressed. E-mail: rohrer@cmu.edu.

- (1) Osterloh, F. E. *Chem. Mater.* **2008**, *20*, 35.
- (2) Kitano, M.; Tsumamaru, K.; Anpo, M. *Top. Catal.* **2008**, *49*, 4.
- (3) Kudo, A.; Miseki, Y. *Chem. Soc. Rev.* **2009**, *38*, 253.
- (4) Domen, K. In *Surface Photochemistry*; J. Wiley & Sons: Chichester, U.K., 1996; p 1.
- (5) Brody, P. S. *Solid State Commun.* **1973**, *12*, 673.
- (6) Brody, P. S. *J. Solid State Chem.* **1975**, *12*, 193.
- (7) Fridkin, V. M. *Ferroelectrics* **1984**, *53*, 169.
- (8) Giocondi, J. L.; Rohrer, G. S. *Chem. Mater.* **2001**, *13*, 241.
- (9) Giocondi, J. L.; Rohrer, G. S. *J. Phys. Chem. B* **2001**, *105*, 8275.
- (10) Giocondi, J. L.; Rohrer, G. S. *Top. Catal.* **2008**, *49*, 18.

- (11) Kalinin, S. V.; Bonnell, D. A.; Alvarez, T.; Lei, X.; Hu, Z.; Ferris, J. H.; Zhang, Q.; Dunn, S. *Nano Lett.* **2002**, *2*, 589.
- (12) Hanson, J. N.; Rodriguez, B. J.; Nemanich, R. J.; Gruverman, A. *Nanotechnology* **2006**, *17*, 4946.
- (13) Dunn, S.; Jones, P. M.; Gallardo, D. E. *J. Am. Chem. Soc.* **2007**, *129*, 8724.
- (14) Liu, X.; Kitamura, K.; Terabe, K.; Hatano, H.; Ohashi, N. *Appl. Phys. Lett.* **2007**, *91*, 044101.
- (15) Cardona, M. *Phys. Rev. A* **1965**, *140*, A651.
- (16) Wemple, S. H. *Phys. Rev. B* **1970**, *2*, 2679.
- (17) Kung, H. H.; Jarrett, H. S.; Sleight, A. W.; Ferretti, A. *J. Appl. Phys.* **1977**, *48*, 2463.
- (18) Berglund, C. N.; Braun, H. J. *Phys. Rev.* **1967**, *164*, 790.

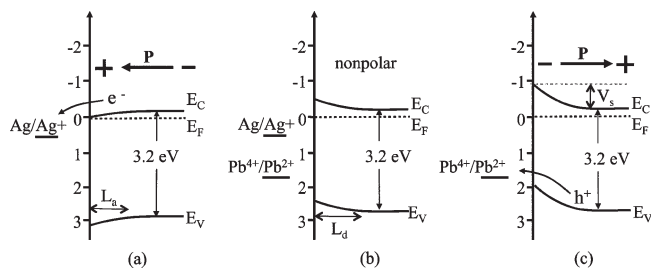


Figure 1. Energy-level diagrams for BaTiO_3 in aqueous solution, without illumination. The energies on the vertical axes are on the standard hydrogen electrode scale. E_V is the valence band edge, E_F the Fermi level, E_C the conduction band edge, V_s the surface potential, L_d the width of the space-charge layer in depletion, and L_a the width of the space charge layer in accumulation. The Ag^+ reduction and Pb^{2+} oxidation reactions are shown at their standard potentials. Images show band bending (a) for a positive domain, (b) for a neutral domain, and (c) for a negative domain.

While the diagrams in Figure 1 suggest an explanation for the spatial selectivity of Ag reduction and Pb oxidation, we are not certain of the amounts of band bending and how this affects the reactivity. A simple hypothesis is that the surface reactivity is due to photogenerated charges in the space-charge region and that the relative reactivity will be related to the width of this region. In this case, any factors that influence the band bending, such as the magnitude of the polarization in the domain, the carrier density, or the dielectric constant, are also expected to influence the reactivity. For example, when illuminated, the density of charge carriers is increased and the width of the space-charge region shrinks. Recent studies of photochemical silver reduction on the surface of lead zirconate titanate indicate that if the energy and flux of the illumination is great enough, silver can also be reduced on negative domains, although at a smaller rate.¹³ This is believed to occur when the concentration of photogenerated charge carriers is great enough to flatten the conduction band.¹³

Note that electrostatic effects of the polarization are not the only factors that influence photocatalytic reactivity. The orientation of the surface has also been shown to be influential in the rate of reactivity on SrTiO_3 ^{19,20} and BaTiO_3 .¹⁰ Also, studies of molecular adsorption on polar lithium niobate surfaces show that the adsorption energy depends on the polarity of the surface.²¹

The purpose of this paper is to describe the relative photochemical reactivity of $\text{Ba}_{1-x}\text{Sr}_x\text{TiO}_3$ solid solutions. In this solid solution series, there are dramatic changes in the magnitude of the polarization and the dielectric constant, both of which influence the width of the space-charge region. Pure BaTiO_3 is a tetragonally distorted, ferroelectric perovskite, and pure SrTiO_3 is a cubic, nonferroelectric perovskite. The photochemical reactions between these compounds and silver have been described previously.^{8–10,19,20} As SrTiO_3 is added to BaTiO_3 , the polarization decreases until it disappears completely at the composition where the tetragonal structure transforms to

a cubic structure. Therefore, the width of the space-charge region in Figure 1a is expected to decrease as SrTiO_3 is dissolved in BaTiO_3 . However, the dielectric constant is also a strong function of composition and maximizes at the tetragonal-to-cubic transition.²² This is expected to increase the width of the space-charge region. To determine how these changes affect the reactivity, the amounts of silver photochemically reduced by $\text{Ba}_{1-x}\text{Sr}_x\text{TiO}_3$ samples with different compositions were evaluated by atomic force microscopy (AFM) and compared. The results are consistent with the banding model for the photochemical reactivity of ferroelectrics.

2. Experimental Methods

Cylindrical, polycrystalline pellets of $\text{Ba}_{1-x}\text{Sr}_x\text{TiO}_3$ in the composition range of $0 \leq x \leq 1$ were synthesized by conventional powder processing techniques from BaTiO_3 (99.7%, Alpha Aesar) and SrTiO_3 (99.9%, Alpha Aesar). Appropriate amounts of the two starting materials were mixed and pellets were formed by pressing the powders (with a few drops of ethanol as a binder) in a 1-cm-diameter cylindrical die with a uniaxial load of 230 MPa. The pellets were then degassed at 900 °C in air for 10 h and then reacted in air at 1250 °C for 12 h. After reaction, the pellets were pulverized; powder X-ray diffraction (XRD) was used to verify that they were single-phase solutions that had structures consistent with previous work.²³ The powders were then ball milled using yttria stabilized zirconia balls to break up hard agglomerates. New pellets were formed from the milled powders, heated at 1280 °C for 10 h, and then 1400 °C for 3 h, all in air. This resulted in relatively dense ceramic polycrystals with grain sizes in the 10–40 μm range. The samples were then ground with sequentially smaller abrasives until a final polish using 0.02- μm colloidal silica. To make grain boundaries easily visible, the sample was thermally etched for 4 h in air at 1225 °C. The visible grain boundaries made it possible to locate the same area of the surface before and after the reaction.

AgNO_3 (Fisher Scientific) was dissolved in deionized water to make a 0.115 M aqueous solution. Similarly, $\text{Pb}(\text{C}_2\text{H}_3\text{O}_2)_2$ (Fisher Scientific) was dissolved in deionized water to make a 0.0115 M solution. An O-ring was placed on the sample surface and filled with the silver- or lead-bearing solution. Light from a 300-W mercury lamp, directed through a fiber-optic light pipe directly above the solution, was used to illuminate each sample. For the Pb oxidation reaction, the exposure period was 3 min. Under these conditions, it is known that Pb^{2+} is oxidized to Pb^{4+} and insoluble PbO_2 is deposited.^{24,25} Exposures for the silver reduction reaction were between 3 and 6 s. For experiments in which the amount of silver was quantitatively compared, exposures of 6 s were used. Under these conditions, Ag^+ is reduced to Ag, which is insoluble.^{26,27} The solid silver deposit forms at the site of reaction. After each reaction, the O-ring was removed, and the sample was washed in water and dried in air.

Topographic AFM and surface potential microscopy (SPM) images were obtained in noncontact mode using a Veeco Digital Instruments Model Dimension 3100 AFM system. Contact AFM images were also obtained using a Veeco Digital Instruments Model CP-II system. Representative regions were imaged

(19) Giocondi, J. L.; Rohrer, G. S. *J. Am. Ceram. Soc.* **2003**, *86*, 1182.

(20) Giocondi, J. L.; Salvador, P. A.; Rohrer, G. S. *Top. Catal.* **2007**, *44*, 529.

(21) Yun, Y.; Altman, E. I. *J. Am. Chem. Soc.* **2007**, *129*, 15684.

(22) Nowotny, J.; Rekas, M. *Key Eng. Mater.* **1992**, *66–67*, 45.

(23) Basmajian, J. A.; DeVries, R. C. *J. Am. Ceram. Soc.* **1957**, *40*, 373.

(24) Tanaka, K.; Harada, K.; Murata, S. *Solar Energy* **1986**, *36*, 159.

(25) Torres, J.; Cervera-March, S. *Chem. Eng. Sci.* **1992**, *47*, 3857.

(26) Clark, W. C.; Vondjidis, A. G. *J. Catal.* **1965**, *4*, 691.

(27) Herrmann, J.-M.; Disdier, J.; Pichat, P. *J. Catal.* **1988**, *113*, 72.

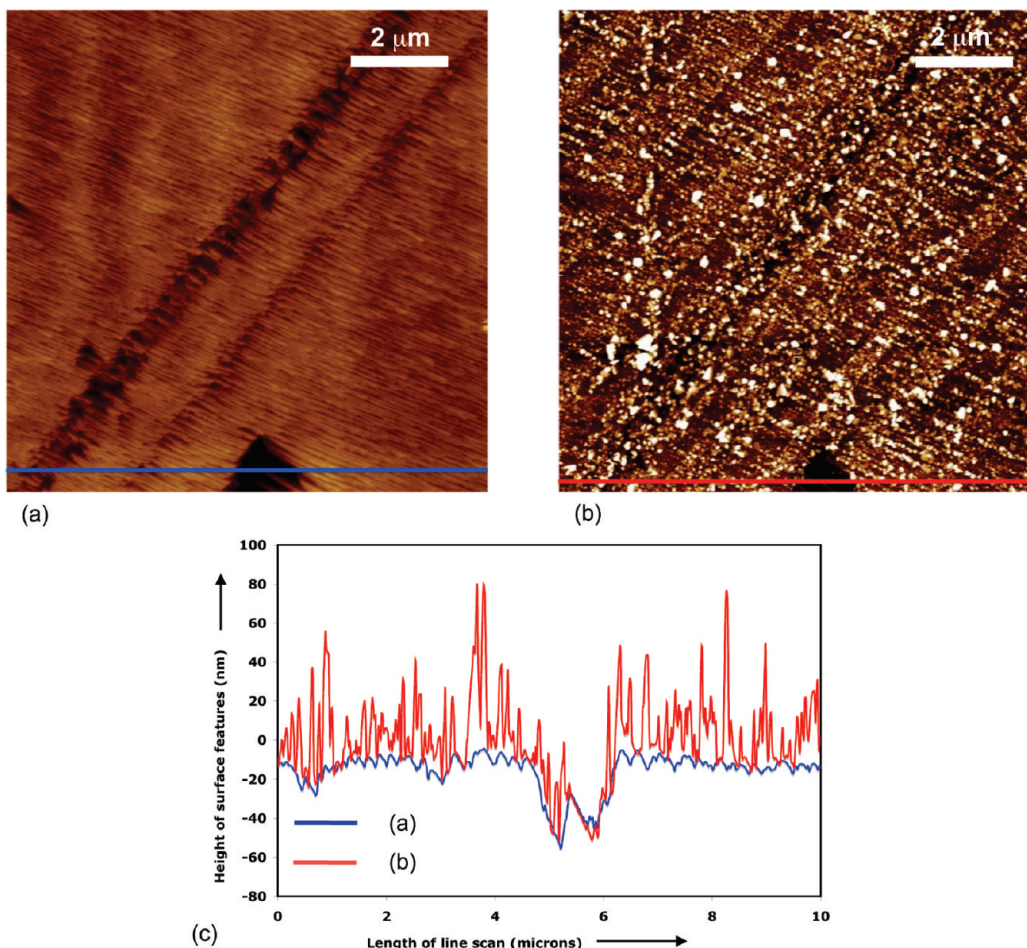


Figure 2. (a) Topographic AFM image of the surface of $\text{Sr}_{0.27}\text{Ba}_{0.73}\text{TiO}_3$ before reaction. The black-to-white contrast is 60 nm. The dominant contrast in this image arises from facets, scratches, and pores. (b) The topographic AFM image of the surface of $\text{Sr}_{0.27}\text{Ba}_{0.73}\text{TiO}_3$ after reaction with AgNO_3 . The black-to-white contrast is 75 nm. Deposited Ag appears as white contrast. (c) Comparison of the surface height profile along the lines in (a, blue trace) and (b, red trace).

before and after the reactions. Several methods were used to estimate the amount of silver on the surface. The most direct method is to compare height profiles recorded at the same location on the surface before and after reaction. An example of this method is illustrated in Figure 2. First, line profiles are obtained from the surface before and after the reaction. The profiles are obtained from near the same location on the two images using natural fiducial marks such as pits and grain boundaries. The two profiles are then plotted together and adjusted along the vertical axis so that the fiducial features coincide. The difference between the areas under the curves, referenced as the excess area, is then taken as a relative measure of the amount of silver deposited by the reaction.

Three pairs of $20\ \mu\text{m} \times 20\ \mu\text{m}$ before and after images were recorded of each sample at randomly selected locations. Four $20\ \mu\text{m}$ line scans were extracted from each image pair so that for each composition, there are 12 measurement of the excess area associated with the silver. These measurements were used to compute an average and standard deviation for the excess area at each composition. Samples with compositions $x = 0.1, 0.2, 0.26, 0.27, 0.28, 0.4,$ and 1.0 were examined in this way.

3. Results

The spatially selective reactivity of the BaTiO_3 surface is illustrated by the images in Figure 3. A topographic image of the surface before any reaction shows two

grains, separated by a grain boundary (Figure 3a). The grain on the left is faceted so that the parallel lines correspond to sets of parallel steps. The surface potential image in Figure 3b, recorded at the same time as Figure 3a, shows wavy lines (corresponding to 180° boundaries) and straight lines (corresponding to 90° boundaries). It was shown by Kalinin et al.²⁸ that regions with a negative potential (dark contrast) correspond to positive domains (those with a component of the polarization perpendicular to and directed away from the surface) while regions of positive potential are negative domains. The apparent reversal of the potential occurs because it is actually the screening charge of the surface adsorbate layer that is sensed in the potential image, not the domain.²⁸ The sample was then used to reduce silver and the image after the reaction is shown in Figure 3c. The silver (white contrast) is clearly concentrated on areas with negative potential in Figure 3b, which correspond to the positive domains. There is a noticeable enhancement in the amount of silver deposited at the boundaries between 180° domains (see Figure 3c). Similarly, silver reduction on LiNbO_3 has been observed to occur only on domain boundaries, and

(28) Kalinin, S. V.; Johnson, C. Y.; Bonnell, D. A. *J. Appl. Phys.* **2002**, *91*, 3816.

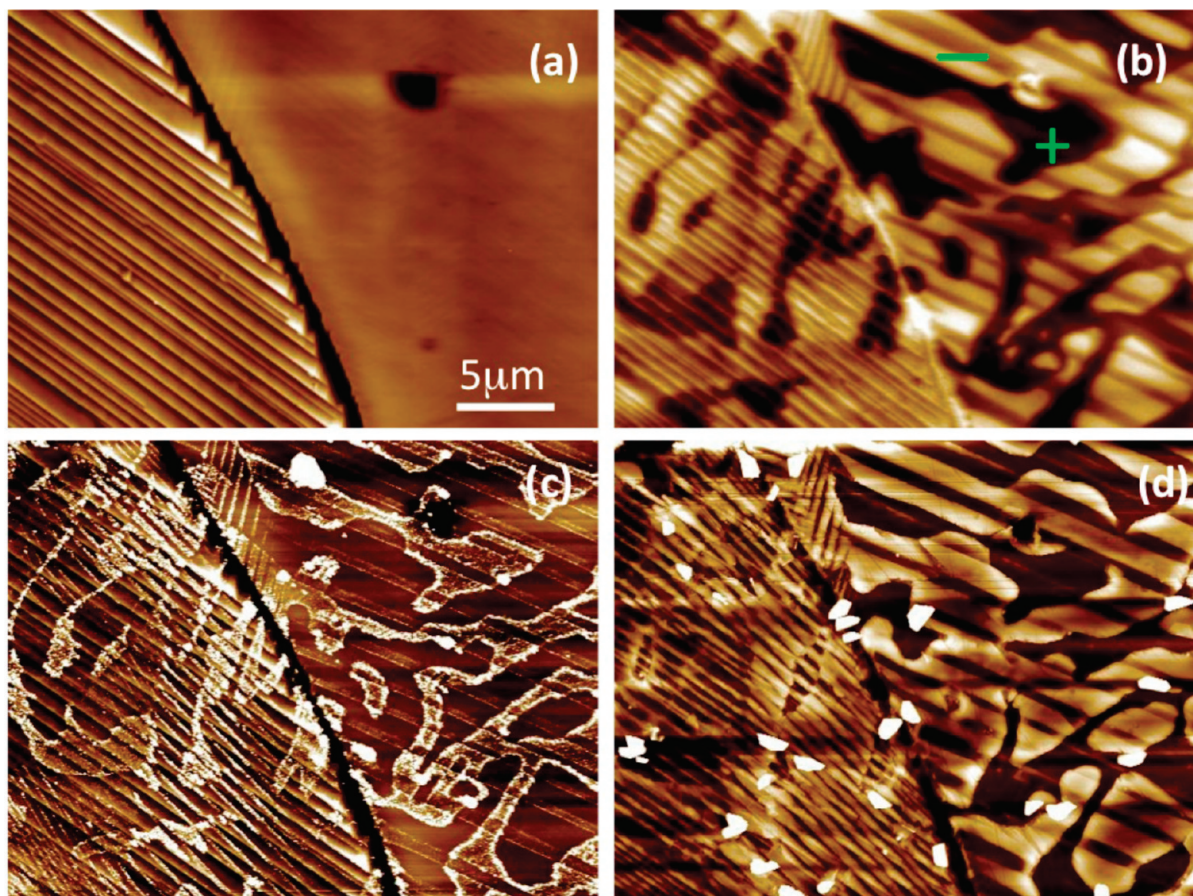


Figure 3. (a) Topographic AFM images of BaTiO₃ surface before reaction and (b) a surface potential image recorded at the same time. (c) Topographic image after reaction in a silver nitrate solution for 3 s. (d) Topographic image after reaction in a lead acetate solution for 3 min. The black-to-white contrast in the images shown in panels (a), (b), (c), and (d) are 100 nm, 175 mV, 60 nm, and 60 nm, respectively.

this has been attributed to inhomogeneous polarization that creates an enhanced electric field at the boundary.¹² A similar mechanism is probably responsible for the current observations. After removing the silver, the sample was used to oxidize lead, and the same area was imaged. In Figure 3d, the white contrast is associated with PbO₂ and it has deposited on the regions with positive potential, which correspond to the negative domains.

A selection of AFM images recorded after the reactions on Ba_{1-x}Sr_xTiO₃ samples are shown in Figure 4. The white contrast in the images corresponds to deposited silver. For the sample with $x = 0.2$ (Figure 4a), the silver is concentrated in stripes, similar to some of the features on pure BaTiO₃ in Figure 3c. Note that the selectivity for silver reduction in active versus inert domains is essentially 100% for pure BaTiO₃ but decreases as strontium is added. For the samples with increasing strontium content, the selectivity is difficult to quantify, because differences in the orientation of the polarization vector, with respect to the surface in different domains and grains lead to significant variations. For the sample with $x = 0.26$ (Figure 4b), which was the most reactive sample, silver deposits everywhere on the surface. It is difficult to distinguish the domain pattern, but there seem to be stripes with more or less silver in the vertical direction. For the sample with $x = 0.27$, the spatially localized reactivity is observed at some locations (as illustrated by

the image in Figure 4c), but not at others. For the sample with $x = 0.4$, the reactivity is spatially uniform at all locations (Figure 4d). Note that the faintly visible continuous lines of contrast in Figure 4d result from residual scratches introduced during polishing.

To clarify whether or not spatially selective reactivity was present on the sample with $x = 0.26$, a second experiment was conducted with a shorter exposure (4 s). The images in Figure 5 show one example from the experiment. The topographic image in Figure 5a shows two grains separated by a grain boundary. A scanning potential image is shown in Figure 5b. The striped contrast on the left-hand grain is characteristic of the potential patterns caused by 90° ferroelectric domains. In the topographic image of the surface after the reaction in Figure 5c, the silver is found on most places on the surface, but there is a clear preference for certain areas. Because the preferred areas are arranged in a striped pattern as in Figure 5b, it is concluded that residual polarization leads to a weak but observable spatial selectivity.

The results of the silver excess area measurements are compiled in Figure 6. Each point is the mean value of 12 measurements, and the bar represents one standard deviation. The SrTiO₃ sample, the sample with $x = 0.1$, and a sample near the transition composition ($x = 0.26$) have the highest reactivities. The samples closest in composition to the transition at $x = 0.2$ and $x = 0.27$ have the lowest reactivities. Optical measurements of MB degradation by

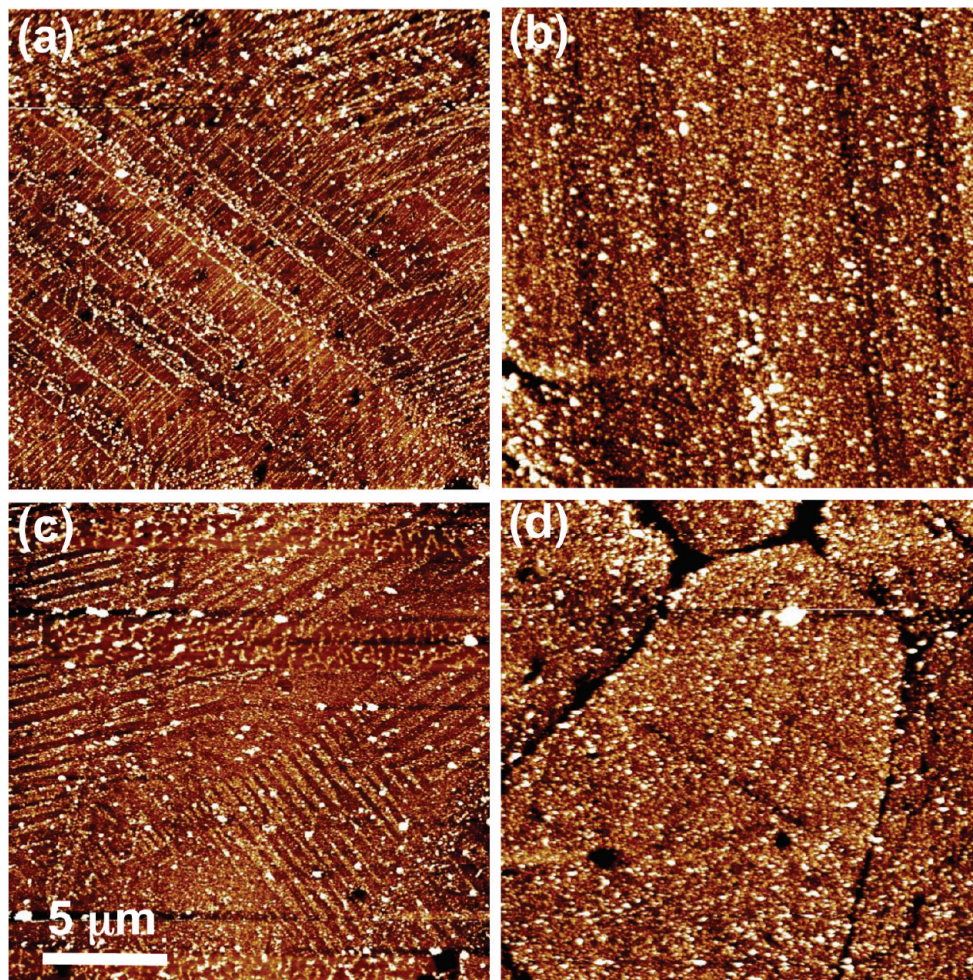


Figure 4. Representative topographic AFM images of four different $\text{Ba}_{1-x}\text{Sr}_x\text{TiO}_3$ compositions after reaction with silver: (a) $x = 0.2$, the black-to-white contrast is 95 nm; (b) $x = 0.26$, the black-to-white contrast is 60 nm; (c) $x = 0.27$, the black-to-white contrast is 60 nm; and (d) $x = 0.4$, the black-to-white contrast is 110 nm. All of the images have a 20- μm field of view.

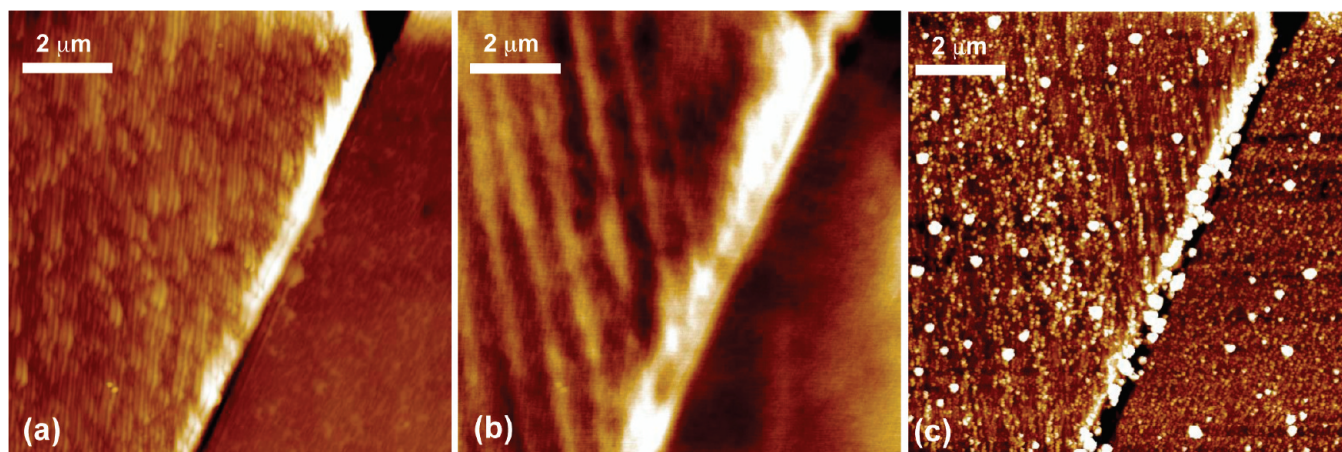


Figure 5. (a) Topographic AFM image of $\text{Ba}_{0.74}\text{Sr}_{0.26}\text{TiO}_3$ surface before reaction and (b), a surface potential image recorded at the same time. (c) Topographic image after reaction in a silver nitrate solution for 4 s. The black-to-white contrast in the images shown as (a), (b), and (c) are 80 nm, 90 mV, and 80 nm, respectively.

similar materials with the same compositions also showed a maximum reactivity at the transition composition.²⁹

4. Discussion

There are several physical parameters that change with the composition of $\text{Ba}_{1-x}\text{Sr}_x\text{TiO}_3$ solid solutions and

might influence the reactivity. At the outset of the discussion of these parameters, a few points and assumptions should be noted. First, while the experiments probed the

(29) Bhardwaj A.; Burbure, N. V.; Rohrer, G. S. Submitted to J. Am. Ceram. Soc., 2010.

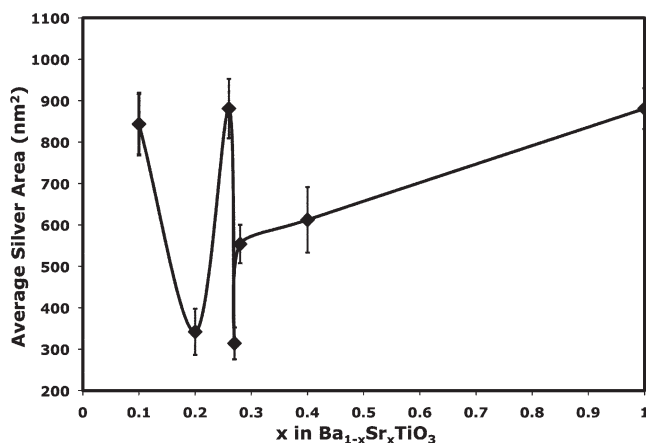


Figure 6. Excess area of silver on the different Ba_{1-x}Sr_xTiO₃ samples. Each point is the mean value of 12 measurements and the bar represents one standard deviation. The line is added only as a guide to the eye.

reduction half of the reaction $\text{Ag}^+ + \text{e}^- = \text{Ag}^0$, the oxidation half of the reaction is constrained by charge neutrality to proceed at the same rate. Holes oxidize water in the charge compensating half of the silver reduction reaction.²⁷ Second, it is assumed that it is principally the charge carriers generated in the space charge regions (see Figure 1) that participate in the surface photochemical reactions. Carriers generated deeper within the bulk of the material have further to diffuse to reach the surface and, because there is no local field to separate the carriers, they are more likely to recombine. Third, the absorption depth is much larger than the space-charge width. The absorption coefficients of BaTiO₃ and SrTiO₃ have been measured near the band edge.^{18,30} Based on these results, the expected absorption depths are on the order of 10² μm, while the space charge width is not expected to greatly exceed 10² nm. Therefore, even though the exact size of the space-charge region is expected to vary with composition, because of ferroelectric domain polarization and other physical parameters, it can be assumed that electron–hole pairs are generated throughout the entire region.

With these conditions and assumptions in place, it follows that anything that increases the space-charge width will make more photogenerated carriers available for the reaction and, therefore, has the potential to increase the reactivity. The width of the space-charge region in depletion (L_d) or accumulation (L_a) can be written as a function of the Debye length, L_D , and the surface potential, V_s .³¹

$$L_d = \left(\frac{2eV_s}{kT} \right)^{1/2} L_D \quad (1)$$

$$L_a = \sqrt{2} \left(1 - \exp \left[\frac{eV_s}{2kT} \right] \right) L_D \quad (2)$$

In eqs 1 and 2, e is the electron charge, k the Boltzmann constant (in units of eV/K), and T the absolute temperature. The surface potential depends on several factors, including the domain polarization, the solution composition, the position of the conduction band edge, and adsorption on the solid surface. Therefore, it is very difficult to define accurately. In fact, for the case of the ferroelectric sample, it is implicitly assumed that the surface potential varies from location to location on the sample surface, as depicted in Figure 1. The Debye length, on the other hand, is a characteristic of the sample and is dependent on the dielectric constant and donor concentration according to eq 3:³¹

$$L_D = \left(\frac{\epsilon_0 \epsilon_r kT}{e^2 N_D} \right)^{1/2} \quad (3)$$

where ϵ_0 is the permittivity of free space, ϵ_r the dielectric constant, and N_D is the donor density. We do not know the donor density of our samples, but Remieka reported a value of $3 \times 10^{19}/\text{cm}^3$ for BaTiO₃.³² Assuming this value for our samples, and taking the dielectric constants for BaTiO₃ and SrTiO₃ to be 1250 and 220,²² respectively, we find that the Debye lengths are 7.7 and 3.2 nm, respectively. Because the donor density is not known, these figures should be considered order-of-magnitude estimates. Throughout the remainder of the discussion, we will consider how changes in the physical parameters influence the Debye length and the surface potential separately.

First, there are clearly changes in the polarization as a function of composition and this affects the surface potential, but not the Debye length. The polarization of BaTiO₃ at room temperature is $26 \mu\text{C}/\text{cm}^2$.³³ As the temperature is increased, it is relatively constant and then decreases precipitously as the Curie temperature is approached.³⁴ Low-temperature polarization data, reported by Hilton and Ricketts,³⁵ indicated that the polarization decreases by ~15% as the strontium content increases from $x = 0$ to 0.3. After the cubic-to-tetragonal phase transition, the polarization is zero. To interpret the present results, the composition dependence of the room-temperature polarization is of interest. Room-temperature data reported by Ianculescu et al.³⁶ indicate that the polarization decreases by ~1/3, from 26 to $17.5 \mu\text{C}/\text{cm}^2$, as the Sr content increases from $x = 0$ to $x = 0.3$. Decreasing polarization in both domains will decrease the surface potential and this will decrease the width of the space charge region, which should decrease reactivity. Except for the point at $x = 0.26$, this agrees with the overall trend. For larger values of x , the polarization decreases precipitously and disappears.

(30) Noland, J. A. *Phys. Rev.* **1954**, *94*, 724.

(31) Monch, W. *Electronic Properties of Semiconductor Interfaces*; Springer-Verlag: New York, 2004.

(32) Remieka, J. P. *J. Am. Chem. Soc.* **1954**, *76*, 940.

(33) Merz, W. J. *Phys. Rev.* **1953**, *91*, 513.

(34) Merz, W. J. *Phys. Rev.* **1949**, *76*, 1221.

(35) Hilton, A. D.; Ricketts, B. W. *J. Phys. D: Appl. Phys.* **1996**, *29*, 1321.

(36) Ianculescu, A.; Mitoseriu, L.; Berger, D.; Ciomaga, C. E.; Piazza, D.; Galassi, C. *Phase Transitions* **2006**, *79*, 375.

Note that the decrease in reactivity between $x = 0.1$ and 0.2 (~60%) is much larger than the decrease in polarization. A second factor that is expected to contribute to a decrease in reactivity with increasing strontium content is solid solution (alloy) scattering. The dissolution of the smaller Sr^{2+} ions creates local distortions in the lattice that can scatter carriers, enhance recombination, and decrease reactivity. This process probably contributes to the decrease in reactivity.

The spatial uniformity of the reduction reaction for samples with $x > 0.27$ is best explained by the absence of polarization in ferroelectric domains. However, assuming that the energy level diagram in Figure 1b is accurate, it is not obvious how electrons surmount the surface potential barrier to reduce silver. Furthermore, it must be recognized that, even before polarization disappears, some silver is found on the surfaces between the positive domains, where there is assumed to be a surface barrier for the electrons. There are two possible ways to explain this. The first is that the surface barrier is not too high, in comparison to the available thermal energy, and electrons occasionally occupy states that allow them to make it to the surface or to tunnel through the barrier. Recall that under illumination, the carrier density will increase and the width of the space charge region will decrease, as discussed by Dunn et al.,¹³ who observed Ag reduction on the negative domains of lead zirconate titanate. The second possibility is that there are surface defects at which the barrier is smaller than the available thermal energy; after silver metal is nucleated at such a defect, the metal semiconductor junction bends the bands in such a way to draw more electrons to this region. After the nucleation event, the situation is analogous to the photochemical diode proposed by Nozik.³⁷ Although the present data do not allow us to distinguish between these possibilities, the uniformity of the observed silver precipitates (for example, see Figure 4d) does not seem consistent with a defect nucleation model. Therefore, the first explanation is more likely.

While the loss of polarization might explain the overall decrease in reactivity from $x = 0.1$ to $x = 0.27$, it does not explain why a local maximum is reached at $x = 0.26$. Among all of the physical characteristics of the sample that change as a function of composition, the only one known to exhibit a singularity at the cubic-to-tetragonal phase transformation is the dielectric constant. Nowotny and Rekas²² cited the dielectric constants of SrTiO_3 and BaTiO_3 to be approximately 220 and 1250, respectively. For all compositions in the $\text{Ba}_{1-x}\text{Sr}_x\text{TiO}_3$ system, there is a sharp maximum in the dielectric constant at cubic-to-tetragonal transition temperature. For example, for $x = 0.3$, the dielectric constant reaches as maximum of 12 500 near room temperature.²² So, for our experiments conducted as a function of composition, we expect the dielectric constant to reach this maximum at the transition composition.

The dielectric constant influences the Debye length and, therefore, the width of the depletion layer (see

eqs 1–3). As the dielectric constant increases, so do the widths of the depletion and accumulation layers. The Debye length changes in proportion to the square root of the dielectric constant. Because the dielectric constant at the transition composition is a factor of 10 higher than other compositions, we therefore expect the space-charge width to increase by a factor of 3.2. The increase in the space-charge width will increase the number of charge carriers that are separated and this should lead to an increase in reactivity. This provides the most reasonable explanation for the local maximum in reactivity at the transition composition.

Another factor that can potentially affect the reactivity is the band gap. However, according to the literature, the bulk band gaps of BaTiO_3 and SrTiO_3 are within a few tenths of a volt of 3.2 eV, so there are not expected to be any abrupt changes. For example, Cardona¹⁵ reported that the band gap of both compounds was 3.2 eV. It can be surmised that the solid solutions would also have gaps close to this value. Other measurements of SrTiO_3 's band gap have yielded values of 3.22 eV,³⁰ 3.17 eV,³⁸ and 3.25 eV,³⁹ so 3.2 eV appears to be a reasonable estimate. With respect to BaTiO_3 , Wemple¹⁶ noted that the optical absorption edge has a tail that makes it difficult to define an exact band gap, but approximates the room temperature band gap to be 3.38 or 3.27 eV, depending on whether the light is polarized parallel or perpendicular to the c -axis, respectively. A later measurement reported 3.29 and 3.14 eV for the same quantities.⁴⁰ Considering these measurements, SrTiO_3 and BaTiO_3 have very similar band gaps, with BaTiO_3 being perhaps 100 mV higher; the band gaps of the solid solution phases have not been determined but can be assumed to be similar to the end points.

The only available band gap data on the solution phases come from thin films.^{41–43} However, these reports are not self-consistent nor are they consistent with the bulk measurements. Thielsch et al.⁴¹ reported that the band gap increases smoothly with the strontium concentration from 3.3 eV to 3.7 eV. Samantaray et al.⁴² also reported a similar smooth increase with strontium content from 3.25 eV to 3.55 eV. Ohara et al.⁴³ reported that the band gap initially decreases with increasing strontium content (from $0 < x < 0.4$), including an abrupt 125 mV step change at the cubic to-tetragonal transition. The grain size, film thickness, and lattice strain can all influence the observed band gaps in these films and this is likely to account for the inconsistency of the reports. Changes in the absorption coefficient should be coupled to changes in the band gaps. Although the absorption

(37) Nozik, A. J. *J. Appl. Phys. Lett.* **1977**, *30*, 567.

(38) Blazey, K. W. *Phys. Rev. Lett.* **1971**, *27*, 146.

(39) van Benthema, K.; Elsässer, C.; French, R. H. *J. Appl. Phys.* **2001**, *90*, 6156.

(40) Hafid, L.; Godefroy, G.; El Idrissi, A.; Michel-Calendini, F. *Solid State Commun.* **1988**, *66*, 841.

(41) Thielsch, R.; Kaemmer, K.; Holzapfel, B.; Schultz, L. *Thin Solid Films* **1997**, *301*, 203.

(42) Samantaray, C. B.; Dhar, A.; Ray, S. K.; Mukherjee, M. L. *Indian J. Phys., A* **2001**, *75A*, 347.

(43) Ohara, K.; Ohsawa, T.; Koinuma, H.; Matsumoto, Y. *Jpn. J. Appl. Phys.* **2006**, *45*, L339.

coefficients for the solid solutions are not known, the absence of evidence for a singularity in band gap energy suggest there is no discontinuous change in the absorption of light at the phase boundary that could account for the local maximum in reactivity.

The position of the conduction band edge is also expected to change with composition, and this is expected to influence reactivity. As the energy difference between the electrons in the conduction band and the silver reduction level increases, the reactivity is expected to increase. Kung et al.¹⁷ reported that, at pH 13.3, the SrTiO₃ conduction band edge is 0.35 V above the BaTiO₃ conduction band edge ($-0.2 \text{ V} \pm 0.1 \text{ V}$ for SrTiO₃ and $0.15 \text{ V} \pm 0.1 \text{ V}$ for BaTiO₃ vs H₂). Electrons at the SrTiO₃ band edge have a larger potential for reducing Ag than in BaTiO₃. The change in the band edge positions, as a function of composition, is not known; however, the band edges should change in a way that is similar to the changes in the band gap.

As a final note, note that Ohara et al.⁴³ recently reported the results of a related experiment. A 50-nm-thick film, compositionally graded in one spatial dimension from pure SrTiO₃ to pure BaTiO₃, was used to reduce Ag⁺ from aqueous solution. X-ray fluorescence was then used to measure the amount of silver, as a function of position along the compositional gradient. The maximum amount of silver was deposited for $x = 0.5$. On both sides of this maximum, the amount of deposited silver decreased until the pure phase was reached. Our results do not span the entire compositional domain, so they cannot be compared between $1 \geq x \geq 0.4$. However, in the

domain of $0.4 \geq x \geq 0.1$, Ohara reported an approximately constant amount of silver, and this did not agree with the present results. While the reasons for this difference is not known, it is likely to be related to the differences between the properties between bulk, macrocrystalline materials studied here and the strained, nanostructured thin film studied by Ohara et al.⁴³ For example, one important difference is that space-charge regions that develop in nanostructured materials are not comparable to those found on the coarse-grained materials described here.⁴⁴

5. Conclusions

The room-temperature photochemical reactivity of Ba_x-Sr_{1-x}TiO₃ solid solutions is spatially selective for compositions with $0 \leq x \leq 0.27$. In this compositional range, the materials are tetragonal. For compositions with $x > 0.27$, the reactivity is spatially uniform. There is a local maximum in the reactivity at the composition $x = 0.26$. This maximum is most likely explained by an anomalously high dielectric constant at this composition that enlarges the space-charge region. The observations reported here are consistent with the space-charge model for the photochemical reactivity of ferroelectrics.

Acknowledgment. The work was supported by the National Science Foundation (through Grant Nos. DMR 0412886 and DMR 0804770). Support from the PA DCED and the National Science Foundation Research Experiences for Undergrads (Grant No. DMR-0648976) is also acknowledged.

(44) Albery, W. J.; Bartlett, P. N. *J. Electrochem. Soc.* **1984**, *131*, 315.